ACS APPLIED MATERIALS & INTERFACES

www.acsami.org

Research Article

Uniform and Stable Aerosol Jet Printing of Carbon Nanotube Thin-Film Transistors by Ink Temperature Control

Shiheng Lu, Joanne Zheng, Jorge A. Cardenas, Nicholas X. Williams, Yuh-Chen Lin, and Aaron D. Franklin*

Cite This: ACS Appl. Mater. Interfaces 2020, 12, 43083–43089

Read Online

ABSTRACT: Semiconducting carbon nanotube (CNT) networks exhibit electrical, mechanical, and chemical properties attractive for thin-film applications, and printing allows for scalable and economically favorable fabrication of CNT thin-film transistors (TFTs). However, device-to-device variation of printed CNT-TFTs remains a concern, which largely stems from variations in printed CNT thin-film morphology and resulting properties. In this work, we overcome the challenges associated with printing uniformity and demonstrate an aerosol jet printing process that yields devices exhibiting a hole mobility of μ_h = 12.5 cm^2/V·s with a relative standard deviation as small as 4% (from over 38 devices). The enabling factors of such high uniformity include control of the CNT ink bath temperature during printing, ink formulation with non-volatile and viscosifying additives, and a thermal treatment for polymer removal. It is discovered that a low CNT ink temperature benefits aerosol jet printing uniformity and stability in both short-term (~1 min) and long-term (~1 h) printing settings. These findings shed light on the effect of a commonly overlooked dimension of CNT aerosol jet printing and provide a practical strategy for large-scale, high-consistency realization of CNT-TFTs.

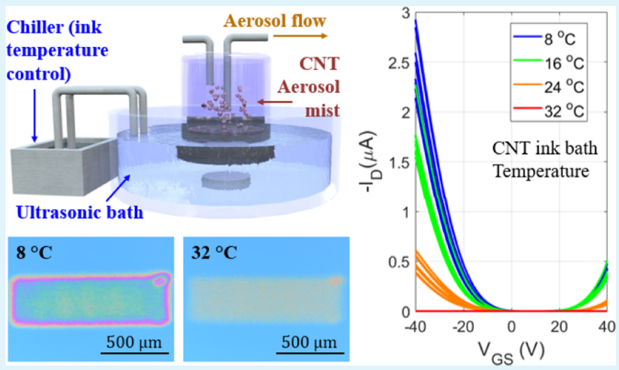

KEYWORDS: *carbon nanotubes, thin-film transistors, aerosol jet printing, device uniformity, ink temperature, printed electronics*

■ INTRODUCTION

Semiconducting carbon nanotube (CNT) thin films are promising for electronics applications because of their superior electrical, chemical, and mechanical properties.[1−4] Their carrier mobility and air stability are high compared to organic semiconductor alternatives;[4] their large surface-to-volume ratio suggests possible implementation in the field of sensing,[5,6] and their mechanical flexibility enables their use in flexible electronics.[7] So far, there have been experimental demonstrations of logic circuits,[8−10] display backplanes,[11] and sensors[4,6] based on the use of CNT thin-film transistors (CNT-TFTs). Among a wide variety of solution-processing techniques, printing has received growing attention for CNT-TFT fabrication because of its low cost and compatibility with a great variety of substrates, both rigid and flexible.[4,7]

While template-based printing (e.g., gravure printing) offers high throughput; direct-write printing, including inkjet printing and aerosol jet printing, has demonstrated potential in rapid prototyping and individual print customization.[12] The recent proliferation of research into printed CNT-TFTs has largely focused on improving printing throughput,[7,12] broadening substrate versatility,[13] expanding applications,[6,14] and enhancing the performance of resulting devices.[15] However, while CNT-TFT wafer-scale uniformity via dip-coating and photolithography has been well-studied,[16,17] there is a lack of studies investigating the performance uniformity of printed devices, even though homogeneity is pivotal for large-scale and practical applications.[18] Limited observations have shown that printing offers inferior device uniformity compared to other CNT deposition methods such as drop-casting or dip-coating.[8,19]

Compared to other direct-write printing methods, such as inkjet printing, aerosol jet printing offers the potential for high process stability,[18] which is a crucial factor influencing device-to-device variation in printed electronics. The incorporated sheath gas flow prevents direct contact between the ink and the nozzle sidewall and thus reduces the risk of clogging (Figure S1),[20] which is a common issue faced by other direct-write methods.[11,12] The relationship between process parameters, such as sheath gas flow rate, and the resulting printed film morphology has been studied for printed conductive Ag and

Received: July 2, 2020
Accepted: August 26, 2020
Published: September 8, 2020

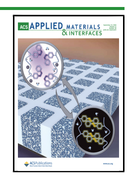

CNT traces, with focus on the impact of flow rates, platen speed, number of printing passes (as illustrated in Figure S2), and platen temperature on film properties and variation.[21,22] Meanwhile, ink temperature, with its strong relationship with the ink rheology properties and volatility,[23] has not been expressly considered.

In this work, we demonstrate an aerosol jet printing process that yields high uniformity and expanded printing stability for CNT thin films in CNT-TFTs. Our devices exhibit transistor performance commensurate with the best previously reported CNT-TFTs, both printed and dip-coated, while achieving the highest device-to-device uniformity. Fine-tuning of the CNT ink bath temperature, an often-overlooked parameter for aerosol jet printing, is one of the key factors enabling the realization of such uniformity. This was achieved by a reduction in the bath temperature from 32 to 8 °C, which improved ink atomization, resulting in an increase in film density and a hole mobility of 12.5 ± 0.5 $cm^2/V \cdot s$. In addition, we found that a lower ink temperature improves short-term (~1 min) printing uniformity and printing stability over the timescale of around 1 h. Other enabling aspects, including ink formulation and the use of rapid thermal annealing (RTA) for polymer removal, also are shown to improve CNT thin-film channel definition and film morphology. These investigations open the door for the direct-write fabrication of highly uniform, wafer-scale CNT-TFTs.

■ RESULTS AND DISCUSSION

The CNT-TFTs explored in this study were fabricated on p++ Si wafers with a 300 nm SiO_2 top layer. As shown in Figure 1a, the devices present a bottom-gate structure with the heavily doped silicon substrate acting as the gate. All other device components were deposited by aerosol jet printing. A detailed description of the printing process is shown in Figure S3 and the Materials and Methods section. As illustrated in Figures 1b and S1, inks containing electronic materials are loaded in an ink vial and atomized into aerosol mists by ultrasonic transduction. The ultrasonic bath is connected to a chiller such that the bath temperature can be precisely controlled throughout the printing process, and the actual ink temperature is tuned correspondingly (Figure 1b). The aerosolized ink is carried by a nitrogen (N_2) gas flow and directed to the deposition head where an annular N_2 sheath flow is applied to focus the aerosol beam for deposition onto the substrate and to prevent direct contact between the ink and the sidewall of the nozzle, which alleviates the risk of nozzle clogging and is thus beneficial for stable printing.[20]

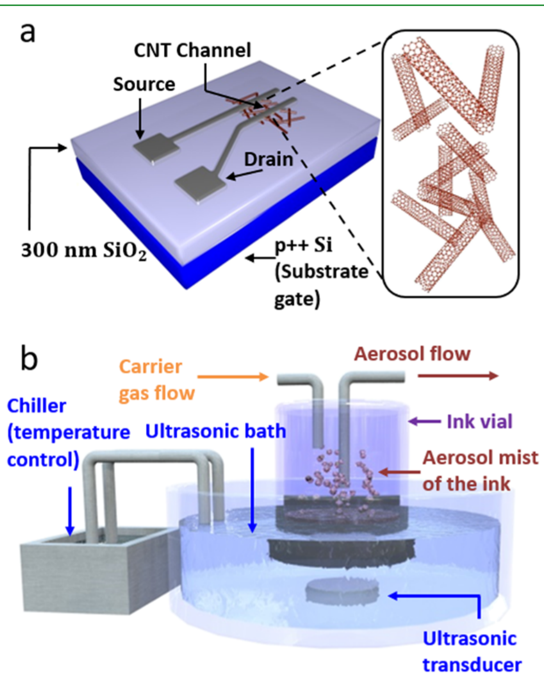

Figure 1. Printed CNT-TFT device structure and aerosol jet printing parameters. Schematic diagrams illustrating: (a) printed CNT-TFT device, including AgNP source/drain contacts, a substrate gate, and semiconducting CNT channel; and (b) an ultrasonic atomizer for the aerosol jet printer (connected to a chiller to control bath and thus ink temperature) used to print the CNT and AgNP thin films.

The CNT ink used in this work was diluted from the commercial semiconducting CNT ink (NanoIntegris IsoSol-S100, 99.9% semiconducting) using toluene; terpineol was added as a secondary solvent. The addition of this viscous, high-boiling point solvent ensures that the microscale ink droplets within the aerosol mist do not dry out before contact with the substrate.[24] It also significantly suppresses the unwanted coffee ring effect commonly observed during the deposition of CNTs either by aerosol jet[22] or inkjet printing,[19] allowing for more continuous CNT films (Figure S4).

In addition to high-boiling point solvent additives, polymer surfactants are frequently used both to separate the semiconducting and metallic nanotubes and to stabilize the dispersion of CNTs in solvents such as toluene. However, once printed, the existence of polymer surfactants in the CNT thin film decreases on-current by screening hole mobility in CNT-to-CNT and CNT-to-electrode junctions.[25,26] The removal of the polymer residue is commonly achieved by annealing,[25,27] solvent rinsing,[28,29] and/or chemical treatments.[26,30] Rinsing and other chemical treatments (including the subsequent drying steps) are possible sources of nonuniformity in printed devices because of their frequent directionality and manual implementation (Figure S5). Hence, when the substrate is compatible, annealing is a more ideal choice as it provides uniform removal of polymer surfactants. The effectiveness of RTA was examined using atomic force microscopy (AFM). As shown in Figure S6, the average nanotube thickness (and diameter) of CNTs drops from ~2.3 to ~1.6 nm after the RTA process, indicating the successful removal of the wrapping polymer. Once the RTA is finished, silver nanoparticle (AgNP) source and drain electrodes were printed atop the CNT channel to complete the fabrication process of the CNT-TFTs.

It is known that exposure of CNT channels to air likely introduces systematic variation in performance among devices,[31,32] which is undesirable for the study of printing-related device consistency. One frequently utilized solution to the negative impact of air-exposed channels is to keep and characterize the devices under high vacuum;[32,33] yet, this considerably increases the measurement complexity and, moreover, is impractical for commercial use. Another option is to deposit a 30 nm Al_2O_3 capping layer on top of the samples using atomic layer deposition (ALD). The capping layer isolates the CNT channels from the ambient conditions, thus minimizing the effects of atmospheric exposure.[31,34] As illustrated in Figure S7, the capping layer introduces ~5× decrease in hysteresis, indicating significantly less interaction with adsorbents from ambient air.

https://dx.doi.org/10.1021/acsami.0c12046
ACS Appl. Mater. Interfaces 2020, 12, 43083−43089

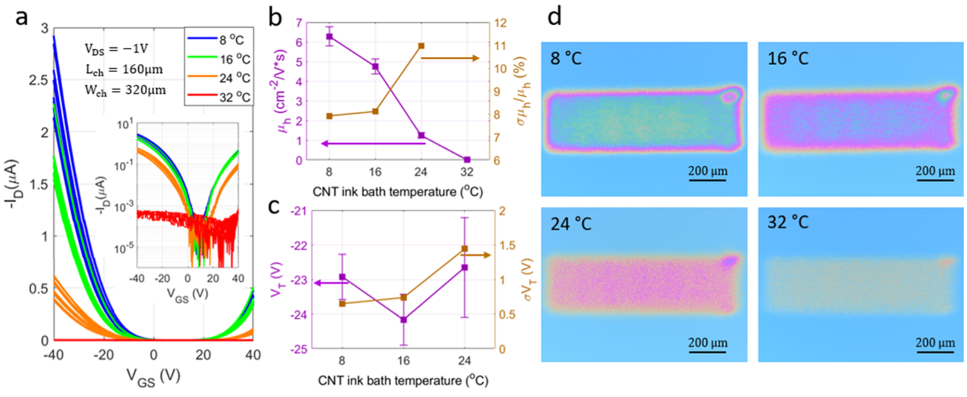

Figure 2. Film morphology and CNT-TFT performance dependence on CNT ink bath temperature. (a) Transfer characteristics and (inset) subthreshold curves of CNT-TFTs as a function of ink bath temperature and characterized in ambient air (devices are covered with 30 nm Al_2O_3 to minimize ambient effects). (b) Mobility (left axis) and the relative variation $\sigma(\mu_h)/\mu_h$ (right axis) as a function of CNT ink bath temperature. (c) Threshold voltage (left axis) and absolute variation $\sigma(\mu_h)$ (right axis), both as a function of CNT ink bath temperature. Each data point represents average ± standard deviation. (d) Optical images of CNT films immediately after printing at different ink bath temperatures.

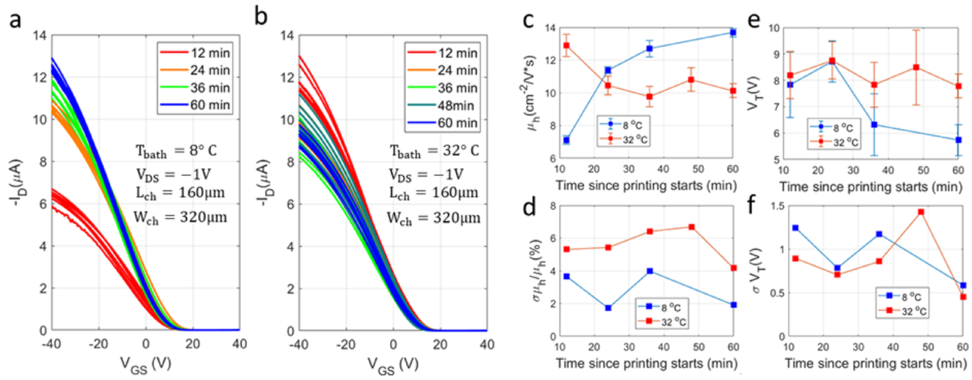

Figure 3. CNT printing stability with respect to ink bath temperature, tested under high vacuum conditions to minimize ambient effects. (a,b) Transfer characteristics of CNT-TFTs printed at ink bath temperatures of 8 and 32 °C, respectively, at various printing durations. Each time point shows 7–8 CNT-TFTs. (c) Mobilities, (d) relative variation of mobility, (e) threshold voltage, and (f) absolute variation of the threshold voltage of CNT channels printed at various time slots at 8 °C (blue) and 32 °C (red).

The electrical performance of the printed TFTs, including the transfer and subthreshold behaviors, are shown in Figure 2a. The TFTs were printed under various CNT ink bath temperatures, while the rest of the printing parameters were the same. It was observed that TFTs printed at lower CNT ink temperatures exhibit higher mobility and larger on-currents (Figure 2a,b), whereas the threshold voltages (V_T) remain relatively independent of the ink temperature (Figure 2c). As shown in Figure S8, TFTs printed at different temperatures exhibit a similar trend in output characteristics at high and low drain/source fields, despite the magnitude of their current being different. This consistency in behavior indicates reasonable consistency in the quality of the CNT/metal contact interfaces, without any notable differences caused by different ink temperatures during printing. The increase in on-current is attributed to higher film density facilitated by increased ink deposition at lower CNT-ink temperatures, as illustrated in Figure S9. Both ink viscosity and surface tension change at different ink temperatures, thus influencing the formation of ultrasonically atomized aerosol.[35] The color variation shown in the optical images of Figure 2d indicates a larger volume of nonvolatile CNT ink components (terpineol, CNTs, and polymer surfactants) transported onto the substrate when printing at lower temperatures. In a CNT film with a randomized network structure, carrier transport is dominated by percolation transport across CNT-to-CNT junctions. Thus, a denser film offers more percolation paths between the source and drain electrodes, giving rise to the higher on-state current and an increased effective field-effect mobility seen in Figure 2a,b.[36,37]

Notably, mobility variation increases as the CNT ink temperature rises. This is pre-eminently caused by a decrease in CNT density with increasing ink temperature. As the CNT density approaches the percolation threshold (below which no conduction path would be available from source to drain), a small change in film density causes a significant shift in performance,[38] which in turn could introduce large variations in mobility from device-to-device. In addition, as the film density increases, the random variations that cause such a significant variance in devices with densities near the percolation threshold are overwhelmed by the already dense CNT films. This is evidenced by examining the CNT-TFTs printed with different numbers of CNT printing passes, which is proportional to the CNT densities. As shown in Figure S10, the relationship between the mobility and the number of CNT printing passes is nearly linear, with the x-intercept close to 1. This suggests that the film density of the 1-pass devices is close to the percolation threshold. Correspondingly, the 1-pass devices exhibit a significantly higher variation in mobility (the standard deviation of mobility $\sigma(\mu_h)$ is close to 100% of the average value) compared to the 2-pass and 3-pass TFTs ($\sigma(\mu_h)/\mu_h$ < 20%).

To further explore the temperature-uniformity dependence, we modified the carrier gas flow rate (18 sccm for 8 °C and 22 sccm for 32 °C) such that the resultant devices achieve similar on-currents and hole mobilities among 67 devices. These devices were printed in intervals to examine the impact of printing time on the resultant uniformity and performance, and the printer was kept operational (printing on dummy wafers without running any pattern files) during the intervals. In an aerosol jet printer, the ink is always printing once the various gas flows are established and stabilized, with a shutter blocking or opening the path between the printed ink and the substrate. Therefore, as the printing time increases, changes in the ink volume and composition are possible because of any number of factors, including inhomogeneous mixing in the ultrasonic bath. As shown in Figure 3, we examined devices printed at the following time points and respective ink bath temperatures: 12, 24, 36, and 60 min at 8 °C and 12, 24, 36, 48, and 60 min at 32 °C. All chips printed at 8 °C, regardless of the time at which printing was performed, have a smaller relative mobility standard deviation (1.9−4.0%) compared to those printed at 32 °C (4.2−6.7%) (Figure 3c,d). This indicates that, over the time scale of printing each set of devices (~1 min for 8 devices), the CNT-TFTs from low-temperature ink exhibit better device uniformity, regardless of mobility and CNT density. Interestingly, threshold voltages and their standard deviations show no apparent relationship to the CNT ink temperature (Figure 3e). While the mechanism remains unclear, the observation nevertheless indicates a promising tendency that the performance uniformity could be considerably enhanced via optimization of the CNT ink temperature.

Interestingly, when printing is carried out for extended periods of time (~1 h), temporal device performance trends vary differently at low and high CNT ink bath temperatures (Figure 3c). At 8 °C, the mobility of the resulting devices tends to rise asymptotically as printing continues, with the most significant variation occurring in the first 30 min of printing. By contrast, the CNT-TFT mobility from devices printed at 32 °C shows a decreasing trend as a function of printing time. Such variation could be explained by examining the amount of ink delivered onto the substrate as the printing proceeds. As shown in Figure S11, at higher CNT ink bath temperature, the volume of the ink delivered onto the substrate tends to decrease throughout the printing process. This phenomenon is attributed to the fact that only a finite amount of CNT ink (~2 mL) is loaded into the atomizer prior to printing and that over time, the ink volume in the atomizer will decrease as a larger fraction of ink is transported to the substrate. As the ink volume in the atomizer drops, less ultrasonically atomized aerosol is generated per unit time, giving rise to lower-density films with a decreased field-effect mobility. However, at 8 °C, the trend reverses, which suggests some factors counterbalance the decreasing ink deposition caused by depletion of the ink volume. If appropriately tuned, ink bath temperature can be utilized to counterbalance the ink volume drop and to realize a steady printing process. The aggressive increase in mobility during the first half-hour of printing is likely due to the three reservoirs (ink, ultrasonic atomizer, and ultrasonic bath) gradually reaching thermal equilibrium, as shown in Figure S12. Therefore, by ensuring all reservoirs have reached thermal equilibrium before printing, the initial rise in mobility can be suppressed (Figure 4). Among the five time points during a 1 h

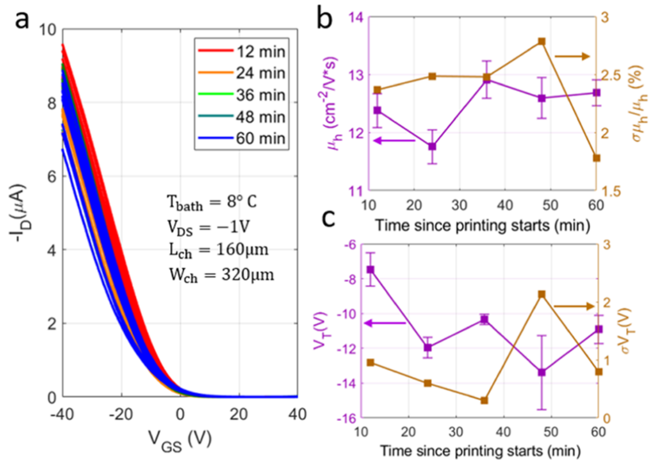

Figure 4. High-uniformity and high-stability printing of CNT-TFTs. (a) Transfer characteristics of printed CNT-TFTs with an ink bath temperature of 8 °C at various printing durations (devices are covered with 30 nm Al_2O_3 to minimize ambient effects). (b) Mobility (left axis) and its relative variation (right axis) of CNT channels printed at various time points. (c) Threshold voltage (left axis) and its absolute variation (right axis) of CNT channels printed at various time points.

CNT printing process, no notable drift in mobility or threshold voltage was observed (Figure 4b,c), and the 38 CNT-TFTs in total yield highly uniform performance, with μ_h = 12.5 ± 0.5 $cm^2/V{\cdot}s$ and $\sigma(\mu_h)/\mu_h$ ~ 4%.

To benchmark the device performance and consistency, a comparison between this work and previous works on CNT-TFTs can be seen in Figure 5.[7,8,11,16−19,39,40] Field-effect hole

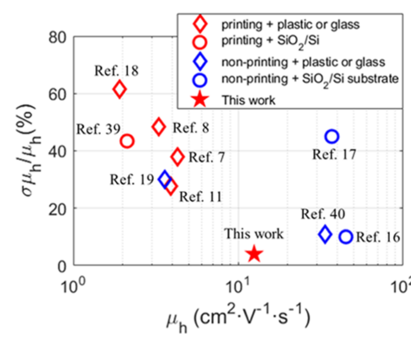

Figure 5. CNT-TFT performance and uniformity benchmarking. Relative standard deviations for hole mobilities of CNT-TFTs plotted with respect to their mobilities. Details for the devices benchmarked in this plot are provided in Table S1.

mobility is chosen as the metric because it is most widely reported in previous works and is extensively studied and discussed in this work. CNT deposition methods and the substrates are also considered because of their potential impact on TFT performance and consistency. Detailed information from all devices is shown in Table S1. In general, while nonprinting techniques, such as drop-casting and dip-coating, offer higher mobilities on average, none of the CNT deposition methods or substrate selections guarantees device-to-device uniformity. The CNT-TFTs realized in this study show a remarkable device-to-device uniformity—better than any of the previous works regardless of the deposition method or the substrate, and a mobility higher than most of the printed CNT-

TFTs and some of the non-printed CNT-TFTs from previous works.

■ CONCLUSIONS

In summary, we discovered that CNT ink temperature plays a significant role in the uniformity of CNT-TFT and the stability of printing nanotube thin films with aerosol jet printing. The combination of proper ink formulation, ink bath temperature optimization, and the polymer removal process gives superior device-to-device uniformity and printing stability. It was discovered that low CNT ink bath temperature (~8 °C) benefits the device consistency in both short-term (~1 min) and long-term (~1 h) printing. It was also observed that the atomization output of toluene + terpineol-based CNT-ink rises at a lower ink temperature. These findings address device consistency issues that have previously plagued printed CNT-TFTs and boost the potential for development of TFT fabrication toward large-scale and high-uniformity production.

■ MATERIALS AND METHODS

Substrate Cleaning and *Poly-L-Lysine* Functionalization. The SiO_2/Si substrates were sonicated in acetone and isopropyl alcohol for 5 min each, rinsed with deionized (DI) water, blow-dried with nitrogen, and they underwent a 3 min oxygen plasma treatment using an Emitech K-1050X plasma asher. The power of the plasma was set to 100 W. The substrate functionalization includes a 5 min immersion in poly-L-lysine solution (0.1 mg/mL, Sigma-Aldrich), DI water rinsing, and nitrogen blow-drying.

CNT Channel Deposition. CNT channels were printed using an Optomec AJ300 aerosol jet printer with a 150 μm nozzle, and 100 μL of 99.9% semiconducting CNT ink (0.1 mg/mL, IsoSol-S100, NanoIntegris), 1900 μL of toluene, and 20 μL of terpineol were loaded into the atomizer sequentially. The sheath flow rate, ultrasonic current, platen motion speed, and platen temperature were set to 30 sccm, 410 mA, 8 mm/s and room temperature (~23 °C), respectively. The carrier gas flow and the ink bath temperature varied. Unless specified, 2 passes of CNTs were printed for the channel.

RTA-Based Polymer Removal. RTA was performed on a Jipelec JetFirst 100 RTA system. Once the sample was loaded, the chamber was purged with nitrogen twice and then was held at a vacuum level of 1 Torr. The chamber temperature was subsequently increased to 450 °C in 2 min, held for 8 min, and cooled down to room temperature within 4 min. The RTA chamber was continuously purged with N_2 during cool-down.

Fabrication of Source and Drain Electrodes. Commercial AgNP ink (UTDAgX, UT Dots Inc.) was used to print the source and drain electrodes. Prior to printing, the ink was mixed with terpineol in a 9:1 volume ratio to modify the ink viscosity, and 2 mL of the as-prepared ink was loaded into the atomizer. Aerosol jet printing of AgNP was carried out using an Optomec AJ300 aerosol jet printer with a 100 μm nozzle. The sheath flow rate, carrier gas flow rate, and ultrasonic current were set to 25 sccm, 18 sccm, and 350 mA, respectively. The platen temperature was held at 60 °C, with a printing speed of 3 mm/s. One pass of AgNP was printed for the electrodes. After printing the electrodes, the samples were placed in an Isotemp 281A oven and baked for an hour at 200 °C under ambient pressure.

Al_2O_3 Deposition. After the fabrication of CNT-TFTs, 30 nm of Al_2O_3 was deposited at 120 °C and 1 Torr using a Kurt Lesker ALD-150LX ALD system. Trimethylaluminum (TMA) was selected as the aluminum precursor, and water vapor was selected as the oxygen precursor. A pulse time of 70 and 40 ms was selected for water vapor and TMA, respectively, and the purge time was 10,000 ms for both precursors and 370 cycles to grow 30 nm Al_2O_3.

Microscopic and Electrical Characterizations. AFM imaging was performed using a Digital Instruments Dimension 3100 AFM. Scanning electron microscopy (SEM) was carried out with an Apreo S SEM from Thermo Fisher Scientific. Electrical characterizations under ambient conditions were performed on a tabletop probe station, and a Lakeshore vacuum probe station was used for electrical characterizations under vacuum ($<10^{-5}$ Torr). Both probe stations were connected to an Agilent B-1500 semiconductor parameter analyzer during the measurements.

■ ASSOCIATED CONTENT

Supporting Information

The Supporting Information is available free of charge at https://pubs.acs.org/doi/10.1021/acsami.0c12046.

Schematic illustrations of the aerosol jet printer working mechanism and the fabrication process flow; ink formulations and the resulting film morphologies; undesirable CNT spread-out due to rinsing; distributions of CNT diameters before and after RTA; additional electrical and microscopic characterizations; and comparison between the performance and consistency achieved in this work and those reported in previous works on CNT-TFTs (PDF)

■ AUTHOR INFORMATION

Corresponding Author

Aaron D. Franklin − *Department of Electrical and Computer Engineering and Department of Chemistry, Duke University, Durham, North Carolina 27708, United States;* orcid.org/0000-0002-1128-9327; Phone: +1-919-681-9471; Email: aaron.franklin@duke.edu

Authors

Shiheng Lu − *Department of Electrical and Computer Engineering, Duke University, Durham, North Carolina 27708, United States;* orcid.org/0000-0002-5323-7787

Joanne Zheng − *Department of Electrical and Computer Engineering, Duke University, Durham, North Carolina 27708, United States*

Jorge A. Cardenas − *Department of Electrical and Computer Engineering, Duke University, Durham, North Carolina 27708, United States;* orcid.org/0000-0002-4403-8962

Nicholas X. Williams − *Department of Electrical and Computer Engineering, Duke University, Durham, North Carolina 27708, United States*

Yuh-Chen Lin − *Department of Electrical and Computer Engineering, Duke University, Durham, North Carolina 27708, United States*

Complete contact information is available at: https://pubs.acs.org/10.1021/acsami.0c12046

Author Contributions

S.L. and A.D.F. designed the experiments. S.L. and J.Z. fabricated the devices and carried out the characterizations. J.A.C. formulated the AgNP ink. Y.-C.L. performed the ALD deposition. S.L., N.X.W., J.A.C., and A.D.F. analyzed the data. A.D.F. supervised the work. S.L. and A.D.F. wrote the manuscript with revision and approval from all authors.

Notes

The authors declare no competing financial interest.

■ ACKNOWLEDGMENTS

This work was supported in part by the Department of Defense Congressionally Directed Medical Research Program (CDMRP) under award number W81XWH-17-2-0045 and by the National Institutes of Health (NIH) under award number 1R01HL146849. This work was performed in part at the Duke University Shared Materials Instrumentation Facility (SMIF), which is a member of the North Carolina Research Triangle Nanotechnology Network (RTNN), which is supported by the National Science Foundation (Grant ECCS-1542015) as part of the National Nanotechnology Coordinated Infrastructure (NNCI).

REFERENCES

(1) Chandra, B.; Park, H.; Maarouf, A.; Martyna, G. J.; Tulevski, G. S. Carbon Nanotube Thin Film Transistors on Flexible Substrates. *Appl. Phys. Lett.* **2011**, *99*, 072110.

(2) Wu, M.-Y.; Zhao, J.; Curley, N. J.; Chang, T.-H.; Ma, Z.; Arnold, M. S. Biaxially Stretchable Carbon Nanotube Transistors. *J. Appl. Phys.* **2017**, *122*, 124901.

(3) Wang, C.; Takei, K.; Takahashi, T.; Javey, A. Carbon nanotube electronics—moving forward. *Chem. Soc. Rev.* **2013**, *42*, 2592−2609.

(4) Chen, K.; Gao, W.; Emaminejad, S.; Kiriya, D.; Ota, H.; Nyein, H. Y. Y.; Takei, K.; Javey, A. Printed Carbon Nanotube Electronics and Sensor Systems. *Adv. Mater.* **2016**, *28*, 4397−4414.

(5) Li, W.-S.; Hou, P.-X.; Liu, C.; Sun, D.-M.; Yuan, J.; Zhao, S.-Y.; Yin, L.-C.; Cong, H.; Cheng, H.-M. High-quality, Highly Concentrated Semiconducting Single-Wall Carbon Nanotubes for Use in Field Effect Transistors and Biosensors. *ACS Nano* **2013**, *7*, 6831−6839.

(6) Andrews, J. B.; Cardenas, J. A.; Lim, C. J.; Noyce, S. G.; Mullett, J.; Franklin, A. D. Fully Printed and Flexible Carbon Nanotube Transistors for Pressure Sensing in Automobile Tires. *IEEE Sens. J.* **2018**, *18*, 7875−7880.

(7) Lau, P. H.; Takei, K.; Wang, C.; Ju, Y.; Kim, J.; Yu, Z.; Takahashi, T.; Cho, G.; Javey, A. Fully Printed, High Performance Carbon Nanotube Thin-Film Transistors on Flexible Substrates. *Nano Lett.* **2013**, *13*, 3864−3869.

(8) Cai, L.; Zhang, S.; Miao, J.; Yu, Z.; Wang, C. Fully Printed Foldable Integrated Logic Gates with Tunable Performance Using Semiconducting Carbon Nanotubes. *Adv. Funct. Mater.* **2015**, *25*, 5698−5705.

(9) Ha, M.; Xia, Y.; Green, A. A.; Zhang, W.; Renn, M. J.; Kim, C. H.; Hersam, M. C.; Frisbie, C. D. Printed, Sub-3V Digital Circuits on Plastic from Aqueous Carbon Nanotube Inks. *ACS Nano* **2010**, *4*, 4388−4395.

(10) Ha, M.; Seo, J.-W. T.; Prabhumirashi, P. L.; Zhang, W.; Geier, M. L.; Renn, M. J.; Kim, C. H.; Hersam, M. C.; Frisbie, C. D. Aerosol Jet Printed, Low Voltage, Electrolyte Gated Carbon Nanotube Ring Oscillators with Sub-5 μs Stage Delays. *Nano Lett.* **2013**, *13*, 954−960.

(11) Cao, X.; Lau, C.; Liu, Y.; Wu, F.; Gui, H.; Liu, Q.; Ma, Y.; Wan, H.; Amer, M. R.; Zhou, C. Fully Screen-Printed, Large-Area, and Flexible Active-Matrix Electrochromic Displays Using Carbon Nanotube Thin-Film Transistors. *ACS Nano* **2016**, *10*, 9816−9822.

(12) Cardenas, J. A.; Catenacci, M. J.; Andrews, J. B.; Williams, N. X.; Wiley, B. J.; Franklin, A. D. In-Place Printing of Carbon Nanotube Transistors at Low Temperature. *ACS Appl. Nano Mater.* **2018**, *1*, 1863−1869.

(13) Lu, S.; Cardenas, J. A.; Worsley, R.; Williams, N. X.; Andrews, J. B.; Casiraghi, C.; Franklin, A. D. Flexible, Print-in-Place 1D-2D Thin-Film Transistors Using Aerosol Jet Printing. *ACS Nano* **2019**, *13*, 11263−11272.

(14) Cai, L.; Zhang, S.; Miao, J.; Yu, Z.; Wang, C. Fully Printed Stretchable Thin-Film Transistors and Integrated Logic Circuits. *ACS Nano* **2016**, *10*, 11459−11468.

(15) Cao, C.; Andrews, J. B.; Kumar, A.; Franklin, A. D. Improving Contact Interfaces in Fully Printed Carbon Nanotube Thin-Film Transistors. *ACS Nano* **2016**, *10*, 5221−5229.

(16) Dong, G.; Zhao, J.; Shen, L.; Xia, J.; Meng, H.; Yu, W.; Huang, Q.; Han, H.; Liang, X.; Peng, L. Large-area and Highly Uniform Carbon Nanotube Film for High-Performance Thin Film Transistors. *Nano Res.* **2018**, *11*, 4356−4367.

(17) Tian, B.; Liang, X.; Yan, Q.; Zhang, H.; Xia, J.; Dong, G.; Peng, L.; Xie, S. Wafer Scale Fabrication of Carbon Nanotube Thin Film Transistors with High Yield. *J. Appl. Phys.* **2016**, *120*, 034501.

(18) Rother, M.; Brohmann, M.; Yang, S.; Grimm, S. B.; Schießl, S. P.; Graf, A.; Zaumseil, J. Aerosol-Jet Printing of Polymer-Sorted (6,5) Carbon Nanotubes for Field-Effect Transistors with High Reproducibility. *Adv. Electron. Mater.* **2017**, *3*, 1700080.

(19) Numata, H.; Ihara, K.; Saito, T.; Endoh, H.; Nihey, F. Highly Uniform Thin-Film Transistors Printed on Flexible Plastic Films with Morphology-Controlled Carbon Nanotube Network Channels. *Appl. Phys. Express* **2012**, *5*, 055102.

(20) Williams, N. X.; Noyce, S.; Cardenas, J. A.; Catenacci, M.; Wiley, B. J.; Franklin, A. D. Silver Nanowire Inks for Direct-Write Electronic Tattoo Applications. *Nanoscale* **2019**, *11*, 14294−14302.

(21) Mahajan, A.; Frisbie, C. D.; Francis, L. F. Optimization of Aerosol Jet Printing for High-Resolution, High-Aspect Ratio Silver Lines. *ACS Appl. Mater. Interfaces* **2013**, *5*, 4856−4864.

(22) Goh, G. L.; Agarwala, S.; Yeong, W. Y. Aerosol-Jet-Printed Preferentially Aligned Carbon Nanotube Twin-Lines for Printed Electronics. *ACS Appl. Mater. Interfaces* **2019**, *11*, 43719−43730.

(23) Seifert, T.; Sowade, E.; Roscher, F.; Wiemer, M.; Gessner, T.; Baumann, R. R. Additive Manufacturing Technologies Compared: Morphology of Deposits of Silver Ink Using Inkjet and Aerosol Jet Printing. *Ind. Eng. Chem. Res.* **2015**, *54*, 769−779.

(24) Rother, M. Engineering of Aerosol-Jet Printed Carbon Nanotube Network Transistors. Dissertation to Obtain the Degree of Doctor of the Natural Sciences, Heidelberg University, Germany, 2019.

(25) Kane, A. A.; Ford, A. C.; Nissen, A.; Krafcik, K. L.; Léonard, F. Etching of Surfactant from Solution-Processed, Type-Separated Carbon Nanotubes and Impact on Device Behavior. *ACS Nano* **2014**, *8*, 2477−2485.

(26) Joo, Y.; Brady, G. J.; Kanimozhi, C.; Ko, J.; Shea, M. J.; Strand, M. T.; Arnold, M. S.; Gopalan, P. Polymer-Free Electronic-Grade Aligned Semiconducting Carbon Nanotube Array. *ACS Appl. Mater. Interfaces* **2017**, *9*, 28859−28867.

(27) Ma, Z.; Han, J.; Yao, S.; Wang, S.; Peng, L.-M. Improving the Performance and Uniformity of Carbon-Nanotube-Network-Based Photodiodes via Yttrium Oxide Coating and Decoating. *ACS Appl. Mater. Interfaces* **2019**, *11*, 11736−11742.

(28) Brady, G. J.; Way, A. J.; Safron, N. S.; Evensen, H. T.; Gopalan, P.; Arnold, M. S. Quasi-Ballistic Carbon Nanotube Array Transistors with Current Density Exceeding Si and GaAs. *Sci. Adv.* **2016**, *2*, No. e1601240.

(29) Dowgiallo, A.-M.; Mistry, K. S.; Johnson, J. C.; Reid, O. G.; Blackburn, J. L. Probing Exciton Diffusion and Dissociation in Single-Walled Carbon Nanotube-C(60) Heterojunctions. *J. Phys. Chem. Lett.* **2016**, *7*, 1794−1799.

(30) Yu, X.; Liu, D.; Kang, L.; Yang, Y.; Zhang, X.; Lv, Q.; Qiu, S.; Jin, H.; Song, Q.; Zhang, J.; Li, Q. Recycling Strategy for Fabricating Low-Cost and High-Performance Carbon Nanotube TFT Devices. *ACS Appl. Mater. Interfaces* **2017**, *9*, 15719−15726.

(31) Ha, T.-J.; Kiriya, D.; Chen, K.; Javey, A. Highly Stable Hysteresis-Free Carbon Nanotube Thin-Film Transistors by Fluorocarbon Polymer Encapsulation. *ACS Appl. Mater. Interfaces* **2014**, *6*, 8441−8446.

(32) Collins, P. G.; Bradley, K.; Ishigami, M.; Zettl, A. Extreme Oxygen Sensitivity of Electronic Properties of Carbon Nanotubes. *Science* **2000**, *287*, 1801−1804.

(33) Noyce, S. G.; Doherty, J. L.; Cheng, Z.; Han, H.; Bowen, S.; Franklin, A. D. Electronic Stability of Carbon Nanotube Transistors Under Long-Term Bias Stress. *Nano Lett.* **2019**, *19*, 1460−1466.

(34) Won Lee, S.; Suh, D.; Young Lee, S.; Hee Lee, Y. Passivation Effect on Gate-Bias Stress Instability of Carbon Nanotube Thin Film Transistors. *Appl. Phys. Lett.* **2014**, *104*, 163506.

(35) McCallion, O. N. M.; Taylor, K. M. G.; Thomas, M.; Taylor, A. J. Nebulization of Fluids of Different Physicochemical Properties with Air-Jet and Ultrasonic Nebulizers. *Pharm. Res.* **1995**, *12*, 1682−1688.
(36) Behnam, A.; Guo, J.; Ural, A. Effects of Nanotube Alignment and Measurement Direction on Percolation Resistivity in Single-Walled Carbon Nanotube Films. *J. Appl. Phys.* **2007**, *102*, 044313.
(37) Snow, E. S.; Novak, J. P.; Campbell, P. M.; Park, D. Random Networks of Carbon Nanotubes as an Electronic Material. *Appl. Phys. Lett.* **2003**, *82*, 2145−2147.
(38) Soliveres, S.; Gyani, J.; Delseny, C.; Hoffmann, A.; Pascal, F. 1/f Noise and Percolation in Carbon Nanotube Random Networks. *Appl. Phys. Lett.* **2007**, *90*, 082107.
(39) Loghin, F.; Colasanti, S.; Weise, A.; Falco, A.; Abdelhalim, A.; Lugli, P.; Abdellah, A. Scalable Spray Deposition Process for Highly Uniform and Reproducible CNT-TFTs. *Flexible Printed Electron.* **2016**, *1*, 045002.
(40) Liang, J.; Tong, K.; Pei, Q. A Water-Based Silver-Nanowire Screen-Print Ink for the Fabrication of Stretchable Conductors and Wearable Thin-Film Transistors. *Adv. Mater.* **2016**, *28*, 5986−5996.

https://dx.doi.org/10.1021/acsami.0c12046
ACS Appl. Mater. Interfaces 2020, 12, 43083−43089